Endoscopic Transplantation of Esophageal Mucosa Grown In Vitro
Using Magnetic Particles in an Externally Administered Magnetic Field

Daniel Manson

May 2012

Abstract

If identified at an early stage, cancer of the esophagus can be removed non-invasively using an endoscope. However, the site of removed tissue rarely recovers completely, and is commonly replaced by a large volume of scar tissue, in some cases causing a significant narrowing of the esophagus. To prevent such post-operative problems it has been proposed that healthy replacement tissue be applied to the site of the cancer, having been grown in vitro from the patient's own cells. In this work we consider one method for improving the adhesion of the new cells to the target site. The method involves seeding the in vitro cells with magnetic particles, and subsequently applying a magnetic force to them using an externally administered permanent magnet, applied for a few minutes during the grafting procedure.

Contents

1 Biological Background

1.1 Gastrointestinal Tract

The gastrointestinal tract (GI tract) is a tube that stretches from the mouth to the anus. The wall of the tube, throughout its entire length, has a fairly constant cross-sectional anatomy consisting of four distinct layers [11]:

Mucus membrane This is the layer on the inner surface (lumenal surface) of the tube and it can be further divided into three sublayers: epithelium, lamina propria, and muscularis interna. The epithelium is arranged into villi and crypts [17], which are made of cells that have a rapid turnover rate - see Figure 1. The lamina propria contains capillaries and lymphatics which supply the epithelium above; and the muscularis interna is a thin layer of smooth muscle.

Submucosa As its name suggests, this layer lies below the mucus membrane. It contains further blood vessels and lymphatics, plus a small number of nerves.

Muscularis propria This consists of longitudinal and circular muscle fibers that together enable the GI tract to act as a pump, moving material down its length, in some cases against the force of gravity.

Adventia This is the outermost layer and consists mostly of connective tissue. Where the GI tract has to move past other parts of the body, the adventia is replaced by a layer known as serosa which contains an epithelium that secretes a lubricating mucus.

Figure 2 shows some of the cell types that are present in these layers. Note that each section of the GI tract has a slightly different selection of cell types, and note also that the basic cross-sectional anatomy is interrupted at various points by macroscopic glands.

1.2 Esophageal Cancer

Cancer can occur at any point in the GI tract; in this work we are specifically interested in the top section: the esophagus, shown in Figure 3. Perhaps the most prominent property of the esophagus is that its inner surface is relatively accessible to an endoscope even though it lies deep in the body. This means that where possible clinicians prefer endoscopic procedures over more invasive ones.

In the US the total number of cases of esophageal cancer is currently around 4.8 per 100,000 persons, with a resulting 4.4 deaths per 100,000 persons. Several distinct cancers occur in the esophagus corresponding to the uncontrolled growth of the various different cell types present. The two most common types are known as squamous carcinoma and adenocarcinoma [4]. The squamous kind occurs in the mucous membrane epithelium, and is the more common of the two. Adenocarcinoma only occurs in patients whose lower esophagus has already changed, becoming more like the lining of the stomach (Barrett's esophagus). In the late nineties the spatial distribution of these cancers in the

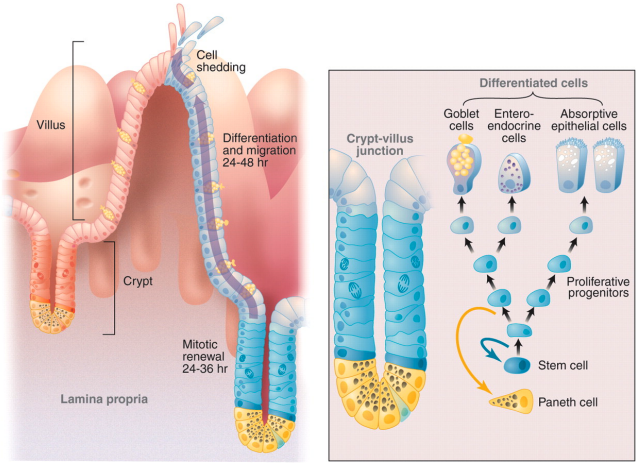

Figure 1: The **left panel** shows the epithelium of the intestine, which consists of deep crypts and tall villi. Each crypt contains a single stem cell that is constantly producing transit amplifying cells, which are very similar to stem cells except for the fact that they can only divide a finite number of times. These cells migrate up the crypt and begin to differentiate according to the tree shown in the **right panel**. At the point they leave the crypt the cells are fully differentiated and capable of performing their function which in most cases involves either secreting or absorbing chemicals. (Paneth cells are secretory cells that remain in the crypt.) On reaching the tip of the villi the death of the cells is triggered.
Taken from [17].

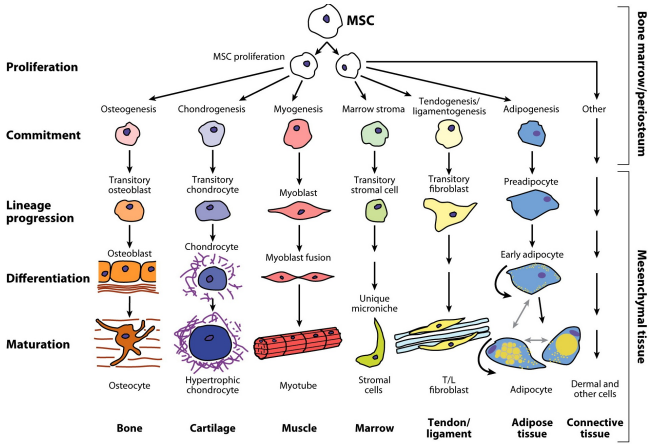

Figure 2: Almost all the cells of the GI tract, except those of the mucus membrane epithelium, derive from mesenchemal stem cells as shown here. Taken from a figure in [20], which was itself adapted from a previously published work.

esophagus was quoted as [25]:

	squamous	adeno-	total
upper third	18%	0%	18%
middle third	45%	0%	45%
lower third	27%	10%	37%
total	90%	10%	100%

However changes in lifestyle appear to be shifting this distribution towards a higher incidence of adenocarcinomas [4]. Indeed smoking and regular alcohol consumption have been shown to correlate with esophageal cancer; obesity and frequent hot beverage consumption may affect risk too. Genetic risk factors do exist but are incredibly rare in the population.

The first symptoms of esophageal cancer generally relate to a problem with swallowing food and liquids. Patients presenting with such symptoms are usually given an esophageal x-ray (using a Barium contrast agent) to check for abnormalities in the shape of their esophagus. They may then be given a positron emission tomography (PET) scan or computed tomography (CT) scan to check for unusual tissue growth elsewhere in the body, i.e. to discover whether the cancer has metastasized. If the cancer is confined to the esophagus the patient's chances of recovery are greater. If this is the case, it becomes appropriate to obtain a more detailed scan of the esophageal cancer, which can be done using endoscopic ultrasonography. For patients with cancer that has penetrated the submucousa and muscularis propria the best option is generally an invasive procedure to cut out an entire section of the esophagus and stitch the remaining two severed ends back together (anastomis) [4]. Of course the length of esophagus that can be removed is severely limited by how far the remaining tissue can safely be made to stretch. The best option, which is only available to patients with the earliest form of the cancer, is to cut out the mucousa using an endoscopic procedure (resection). In fact, the technique required for removing carcinoma in the submucousa (endoscopic dissection) has recently

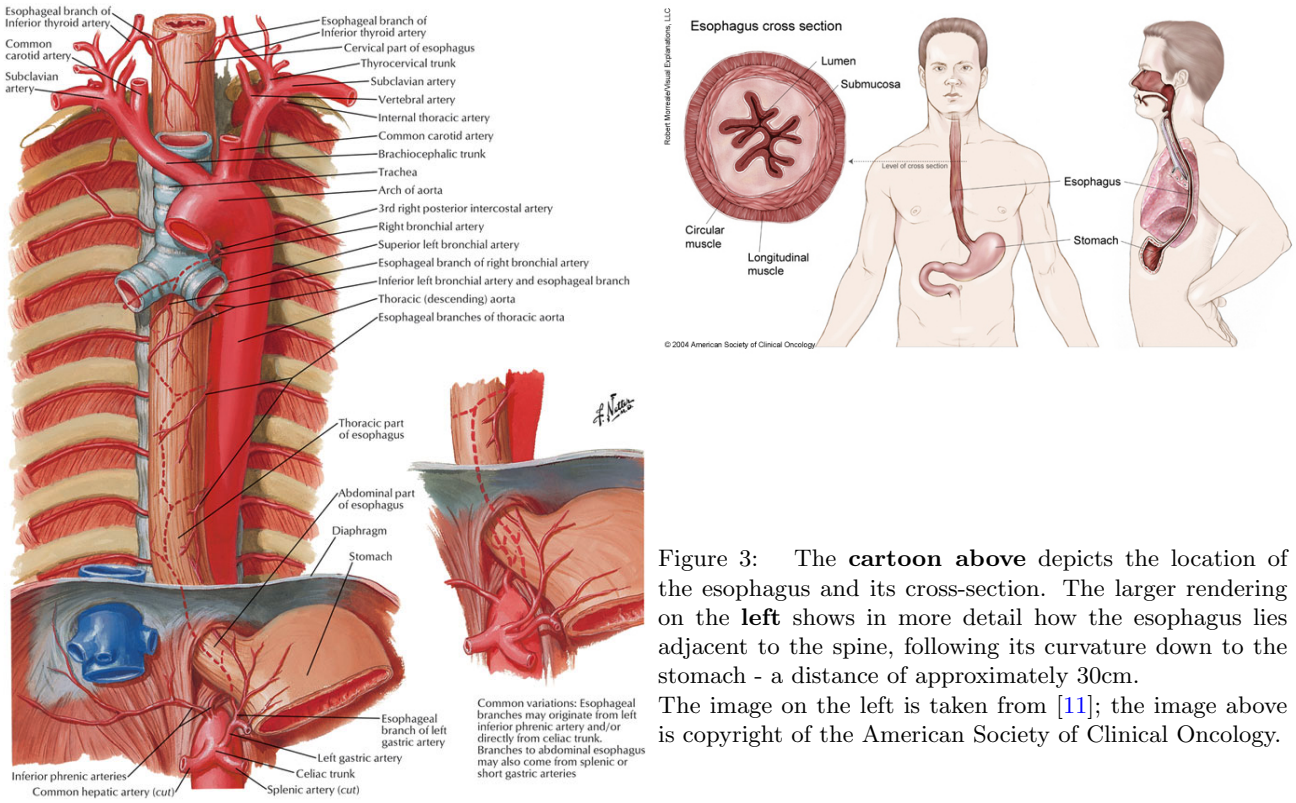

Figure 3: The **cartoon above** depicts the location of the esophagus and its cross-section. The larger rendering on the **left** shows in more detail how the esophagus lies adjacent to the spine, following its curvature down to the stomach - a distance of approximately 30cm.
The image on the left is taken from [11]; the image above is copyright of the American Society of Clinical Oncology.

been improved and it is suggested that this should be used more widely [7]. In both cases, however, invasive surgery is necessary if the cancer is larger than about 3cm.

Patients who have cancerous mucosa and submucousa removed have a good chance of recovery, but the site of tissue removal often develops a large volume of scar tissue which after some time may result in the esophagus becoming blocked (stenosis). This is a problem which may be addressable with tissue engineering; indeed initial trials in dogs have already proven successful [13].

1.3 Tissue Transplants and Tissue Engineering

There are several medical circumstances in which a macroscopic section of tissue is required for a graft. Required tissue types include skin, bone, blood vessel, and GI tract. Sourcing each of these tissues is associated with a set of problems, so where possible tissue is taken from elsewhere in the patient's body (autologous grafting). This prevents the problems associated with an immune response to foreign material, but it may cause other problems if the transferred tissue type is not an exact match [1]. If the patient is incapable of donating to themselves the next best option is generally a donation from a close relative (syngenic grafting), but this will likely produce an immune response.[1] For some grafts it is unethical or inappropriate to take tissue from a relative and so tissue is taken instead from an immunologically matched cadaver (allografting). Prior to the development of tissue engineering, the final transplantation option was to take a donation from another species (xenografting). In an emergency, or if the recipient is not an adult, this can be more convenient than the other options, but it introduces the danger of cross-species viral infections [19] in addition to the immunological problems.[2] As an alternative to transplantation, in some circumstances it is possible to create an artificial implant. However, matching the engineering standards achieved by evolution is not simple, especially when restricted to a set of biologically-compatible materials.

Tissue engineering attempts to overcome the problems associated with transplantation and implantation by growing the patient's own tissue in vitro. In principle, the only problem with this approach is that grafts inevitably take several days to grow and so cannot be provided to the patient in an emergency. However, growing tissue in vitro is not an easy task [16]: the correct cell types must be obtained and isolated; the relevant extracellular signaling molecules must be identified and supplied to the cell culture; and a physical matrix must be supplied to which the cells can adhere appropriately. A more primitive form of tissue engineering partially avoids the first two steps by harvesting a large amount of tissue and dissecting out small sections of suitable material to be inserted directly into the matrix without significant ex vivo culturing [24]. The success of this technique in animal models is encouraging, but it is of little clinical use in itself given the quantity of tissue required.

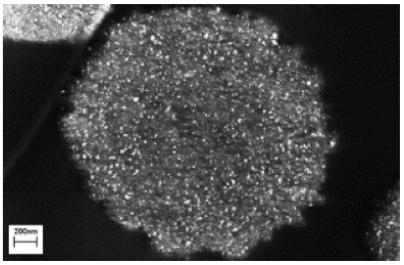

Figure 4: Scanning electron micrograph of an M-280 Dynabead. The bright spots are the nanoparticles. Note that the M-280 beads have slightly different specifications compared to the M-450 beads referred to elsewhere in the text. Figure taken from [5].

[1] If the donor and recipient are genetically identical (i.e. monozygotic twins or clones) the chances of an immune response are much lower.

[2] Non-primate mammals (and New World monkeys) express a particular cell-surface marker that primates' immune systems are very effective at recognizing and reacting to (the α-gal epitope). Indeed as much as 1% of circulating immunoglobulin proteins appear to be selective for this marker [6]. A number of methods for overcoming this problem have been investigated with varying degrees of success, the most notable being the creation of knock-out pigs that do not express the marker in question.

Cells In the case of replacing a section of the airway, it is thought that at least two cell types must be cultured, namely epithelial cells and chondrocytes [12]. However to mask missing mucosa and submucousa in the esophagus one cell type may suffice - oral epithelial mucsoal cells [13]. Isolating a pure sample of cells from a biopsy is a very technical process involving the use of several antibiotics, enzymes and other organic and inorganic solutions. Sometimes it is necessary to cycle the culture through a series of different temperatures. Centrifuges [12], magnetic particles [14] (see next section and Figure 4), and even forceps [13] may also be required. In pre-clinical studies this step can be avoided by using an appropriate commercially available surrogate cell line such as human umbilical vein endothelial cells (HUVECs) [15].

Growth factors The signaling molecules which trigger growth, and in some cases differentiation, can be supplied directly as a solution [23] or generated in situ by a set of 'feeder cells', which come from commercially available cell lines [13]. However, avoiding the use of non-autogenic cells at all phases of the tissue engineering process is preferable.

Matrix The matrix can either be made of a synthetic polymer [8], or of a decellularised piece of collagen [15, 12]. In both cases the material should be resorbable, that is the body should be capable of naturally breaking it down over the course of a few days or weeks. If the graft is to be only one or two layers thick, pre-clinical studies have shown that it is possible to culture it without a matrix, and then transfer it to the in vivo site using a piece of tape, which is only left in the patient for a few minutes while the cells adhere to the target site [13].

If a matrix is used, there are often problems encouraging cells to adhere to it, which makes the fabrication of thick grafts a challenge. Several different designs of bioreactor have been developed to address this issue [16] and to ensure that cell seeding is homogeneous. One approach to reactor design is to try and mimic the physical conditions present at the in vivo site so that any mechanical signaling pathways present in the cell will drive it to adhere [8].[3] In many cases this means cell medium is pumped (perfused) along the axis of the matrix; multiple cell mediums can be pumped along the inside and outside of the graft if necessary [12]. An additional method is to label the cells with microscopic magnetic beads and use a magnetic field to apply a force that drives the cells towards the matrix, thus increasing the probability of them adhering to it [15]. Although this is not the application of magnetic beads discussed in this work, what is considered here is essentially an in vivo implementation of this in vitro technique.

2 Magnetic Beads

It is possible to manufacture nanometer-sized maghemite (γ-Fe_2O_3) particles [5]. These nanoparticles exhibit superparamagnetism which means that the magnetic moments of their constituent atoms are always in alignment (except at very high temperatures) [14] - see Figure 5. Unlike with most materials, when a nanoparticle is placed in an external magnetic field its magnetic moment aligns to the field, even if the field is relatively weak. The ability to easily shift the magnetic moment of the nanoparticles can be exploited in three distinct ways: as a source of thermal energy; as an anomaly in magnetic

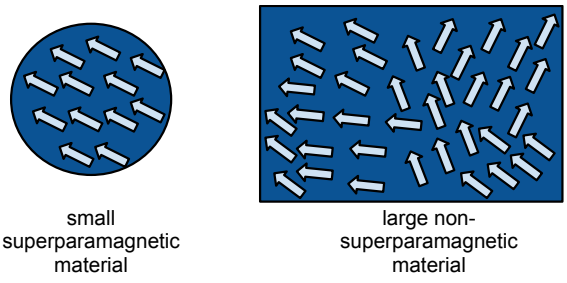

Figure 5: The particle on the **left** is nannometer-sized and thus the magnetic moments of all its atoms are aligned, even in the absence of an external magnetic field. The material on the **right** is larger and has no net magnetization in the absence of an external field.
Note that the nanoparticle is so small that the direction of its 'unanimous' magnetisation vector fluctuates in the presence of thermal energy. These fluctuations, however, are restricted by the anisotropic properties of the particle (such as its crystalline structure and gross asymmetry).

[3] An alternative approach is to directly trigger the mechanosensitive channels in the cells using magnetic particles and a magnetic field (see the following sections in this work for details on applying forces in this way) [14].

resonance imaging (MRI); or as a source of mechanical force. The details and medical applications of these processes are reviewed elsewhere [5]; here we are interested only in the force-generating capacity of the nanoparticles, which is discussed in the next section.

Pure maghemite particles are not particularly useful for medical applications, but they can easily be coated in a bio-compatible polymer [5]. It is also possible to embed multiple particles into micron-sized polymer beads and then coat the beads in a bio-compatible polymer - see Figure 4. Once coated, the beads or particles can have specific molecules attached to their surface so that they bind preferentially to a particular molecule, organelle, or cell type. Figure 8 shows how M-450 Dynabeads can be made to recognize specific cell types.

3 Modeling Magnetism

3.1 Field Around Permanent Magnets

In a system without electric currents or sources and in which magnetic fields are static, we need only consider Gauss' Law for magnetism:

$$\nabla \cdot \mathbf{B} = 0 \tag{1}$$

where $\mathbf{B}$ is the magnetic field. For most materials $\mathbf{B}$ is proportional to $\mathbf{H}$, the externally applied magnetic field, i.e. $\mathbf{B} = \mu_{\text{material}}\mathbf{H}$. However in ferromagnetic materials there is a point at which an increase in $\mathbf{H}$ does not cause a significant increase in $\mathbf{B}$, this is because the atoms in the material approach their magnetic saturation. For such materials it is common to define the relationship between $\mathbf{B}$ and $\mathbf{H}$ using empirically obtained curves, these curves are also used to specify the baseline magnetic field strength of permanent magnets - see Figure 7.

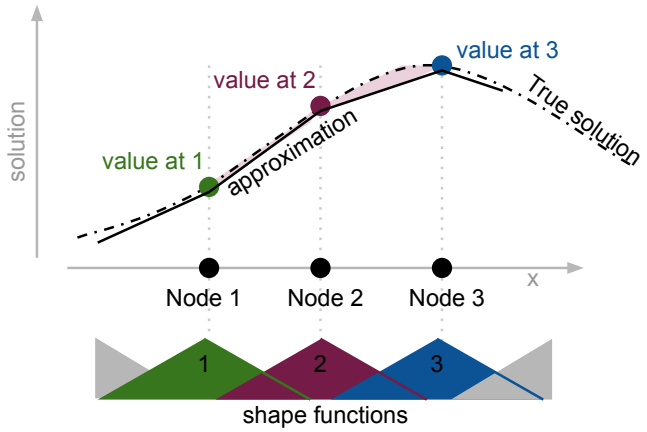

Figure 6: For a linear differential operator D, suppose we want to find an approximate solution to the following equation:

$$D[u(x)] = \rho(x)$$

Here the **dotted black line** is the true (but unknown) solution which we are attempting to approximate. The approximation, shown in **solid black**, consists of a weighted sum of the **three labeled values**, ϕ_i, where the weights are given by the shape functions, N_i, in the **lower** part of the figure.

The **pink shaded region** between the true solution and the approximation corresponds to the error of the approximation. This error cannot be evaluated without knowing the solution, but if we apply the operator D to our approximation we can compare it to $\rho(x)$; the difference between these two values is known as the residual.

To find a good approximation one must minimize the residuals with respect to changes in the three ϕ_i values. But what quantity exactly is to be minimized? In electromagnetism calculations it is common to minimize the integral of the residuals weighted by each shape function, i.e. there are three separate integrals to be minimized:

$$\int N_k(x) \left(\sum_i D[N_i(x)\phi_i] - \rho(x) \right) dx \quad \text{for } k = 1, 2, 3$$

These minimizations can be expressed in matrix form as:

$$K\Phi = S$$

where K is a matrix with elements corresponding to N_k and $D[N_i]$ pairs, Φ is a vector of the ϕ_i and S is a vector corresponding to ρ and N_k. The exact details of these depend on D and in fact it is common to integrate by parts before expressing this minimization in matrix form.

At this point we should be able to apply standard linear algebra to find the solution. However when dealing with non-linear B-H curves we will find that the matrix K depends on the value of the solution, and as a result it becomes necessary to use an iterative approach to finding the solution; the Newton-Raphson method is appropriate so long as the B-H curve is smooth and a good starting value is chosen.

The method outlined thus far does not actually give the final solution: boundary conditions must still be imposed. However, once this is done the solution can be evaluated at any point and used in further calculations as required.

Note that although the example shown here is a one dimensional system, the method generalizes to multidimensional space with potentially hundreds of thousands of nodes.

See the software manual [21] for more details.

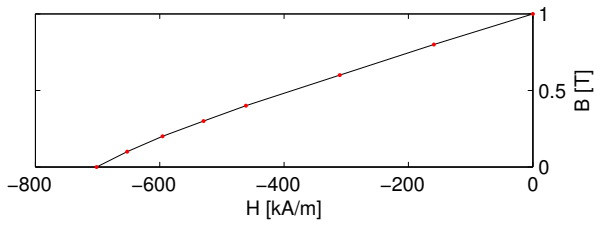

Figure 7: Magnetisation curve for a one Tessla permanent magnet made of a neodymium-boron alloy of iron. Increasing the external magnetic field in the 'wrong' direction reduces the magnetic field in the magnet.

When looking for solutions to Equation 1 it is helpful to define $\mathbf{H}$ in terms of a scalar field, ψ, known as the total scalar potential:

$$\mathbf{H} = -\nabla\psi$$

Thus we arrive at the following equation:

$$\nabla \cdot \mu\nabla\psi = 0 \tag{2}$$

This equation cannot be solved analytically, instead it is approximated by finite element modeling software [22]. This involves splitting the domain into thousands of tetrahedra and approximating the solution around each vertex. Figure 6 explains how this is done in some detail.

3.2 Force on Magnetic Particles

Outside of the permanent magnets, to a good approximation $\mathbf{B} = \mu_0\mathbf{H}$. This is true even in cells with magnetic nanoparticles [5]. Taken together with the fact that the nanoparticles' dipoles, $\mathbf{m}$, align to the magnetic field, we see that the force on the nanoparticles F_m is relatively easy to calculate:

$$\mathbf{F}_m = (\mathbf{m} \cdot \nabla)\mathbf{B} \tag{3}$$

where $\mathbf{m}$ is given by the product of the nanoparticle volume, V_m, and the volume magnetization, $\mathbf{M}$. The calculation of $\mathbf{M}$ is a little more involved [9] but essentially is given by the expectation of the component of the particle's true dipole, μ, in the direction of $\mathbf{H}$. The probability distribution is given by the Boltzmann factor and reflects the relationship between the energy of the dipole in the magnetic field and the amount of thermal energy in the system:

$$M = \mathbb{E}_\theta[\mu\cos\theta] = \int_S \mu\cos\theta\ P(\theta)dS = \int_S \mu\cos\theta\ N\exp\left(\frac{\mu H\cos\theta}{k_B T}\right)dS \tag{4}$$

where S is the surface of a sphere, θ is the angle of the dipole relative to H, k_B is the Boltzmann constant, T is temperature, and N is a normalization factor. It is helpful to express μ as a product

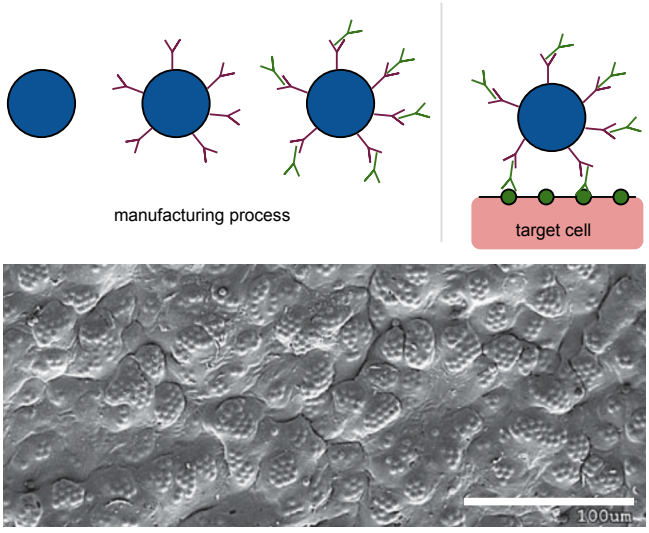

Figure 8: The **top left panel** shows how the M-450 beads are coated in human antibodies that bind specifically to mouse antibodies (human antibodies shown in **red**). Once coated in these antibodies, a second set of antibodies are added. These are mouse antibodies that bind specifically to a particular human cell type (e.g. CD31 or CD29) by recognizing a particular cell surface protein (mouse antibodies and surface proteins shown in **green**). The **top right panel** shows how the beads as a whole bind to the given human cell type. This two-step binding mechanism makes it relatively easy to create a range of classes of beads with different specificities. See the manufacturer's manuals for more details [3].
The **bottom panel** is taken from [15]. It is an SEM image showing M-450 Dynabeads bound to the CD31 cell surface molecule PECAM-1. There are an average of 6 beads per cell.

of the nanoparticle volume, V_p, and its volume magnetic saturation, M_s.[4] Evaluation of the integral gives:

$$M = M_0 \left[\coth\left(\frac{V_p M_s H}{k_B T}\right) - \left(\frac{V_p M_s H}{k_B T}\right)^{-1} \right] \tag{5}$$

where M_0 is the magnetic saturation value for the bead; for free nanoparticles $M_0 = M_s$. Figure 9 shows the relationship between M and B for M-450 Dynabeads at room temperature; note how the magnetization increases dramatically at low field strength and then begins to saturate.

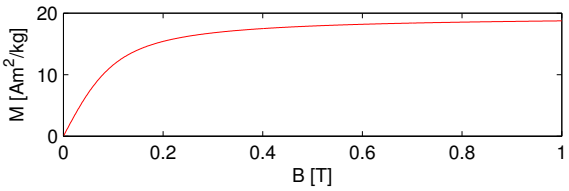

Figure 9: Mass magnetization curve for M-450 Dynabeads at room temperature. Graph generated using Equation 5 and data from [5].

We now introduce χ defined by $\mathbf{M} = \chi\mathbf{H}$ or equivalently $\mathbf{M} = \chi\mathbf{B}/\mu_0$. This simplifies the vector calculus in Equation 3 and we now have:

$$\mathbf{F}_m = \frac{V_m \chi}{\mu_0}(\mathbf{B}\cdot\nabla)\mathbf{B} \qquad \text{where } \chi = \frac{M_0}{H}L(x),\ x = \frac{V_p M_s H}{k_B T},\ \text{and } L(x) = \coth x - x^{-1} \tag{6}$$

Note that L is the Langevin switch function.

4 Magnet and Particle Specification

Following the above discussions, it is now possible to succinctly state the proposal under consideration:

> *Could magnetic particles together with a strong magnetic field be used to aid the adhesion of a sheet of mucosal epithelial cells to a section of exposed submucosa in the esophagus?*

The first step in addressing the numerical feasibility of this proposal is to estimate the distance between the external magnet and the esophagus. Figure 10 depicts a simple ellipse-and-circle model of the thorax and esophagus, and gives an indication of the distances to be expected from a selection of different body sizes. Note that the interior of the esophagus is not usually circular - see Figure 3 - but during endoscopic procedures gas is delivered to inflate (or 'insufflate') it. Note also that the model calculates distance along normals from the surface of the esophagus, since this is the direction in which the force must be applied (unless we intend to use very complex magnetic fields). The dimensions of the thorax have been modeled here because, as was noted in a preceding section, the majority of carcinomas occur in the lower two thirds of the esophagus, i.e. below the neck. Clearly, distances to the skin in the upper third of the esophagus will not be as problematic. The conclusion to be drawn from the figure is that approximately half the esophageal surface lies within 10cm of the skin, but the remaining half may lie as much as 12-18cm away (or more), depending on the patient's dimensions.[5]

[4] Note that this magnetization saturation occurs spontaneously due to being superparamagnetic.

[5] Note that along some stretches of arc the distance to the skin is significantly longer in one direction that in the opposite direction, but we cannot take advantage of this as the forces generated by external magnets can only ever be made to point towards the magnet (except perhaps with a highly complex and specific magnet design). This results from an important property of the vector calculus in Equation 6: the direction of the largest forces cannot be reversed simply by reversing $\mathbf{B}$. To see this, we define $\mathbf{B}(x,y,z) = (B_x(x,y,z), B_y(x,y,z), B_z(x,y,z))$ and consider one component of the vector calculus:

$$[(\mathbf{B}\cdot\nabla)\mathbf{B}]_x = B_x\frac{\partial B_x}{\partial x} + B_y\frac{\partial B_x}{\partial y} + B_z\frac{\partial B_x}{\partial z} \tag{7}$$

here the sign of the first term is independent of the sign of B_x (since two minus signs cancel); i.e. its sign is governed only by the x-derivative of $|B_x|$. The second and third terms in the equation may be affected by the sign of B_x, but this is less important: we can define x as the direction of $\mathbf{B}$, giving B_y and B_z as zero and thus removing the two terms in question (and the $[\cdots]_y$ and $[\cdots]_z$ components will be small since $\frac{\partial B_y}{\partial x}$ and $\frac{\partial B_z}{\partial x}$ ought to be small in the regions where B_x and $\frac{\partial B_x}{\partial x}$ are designed to be large).

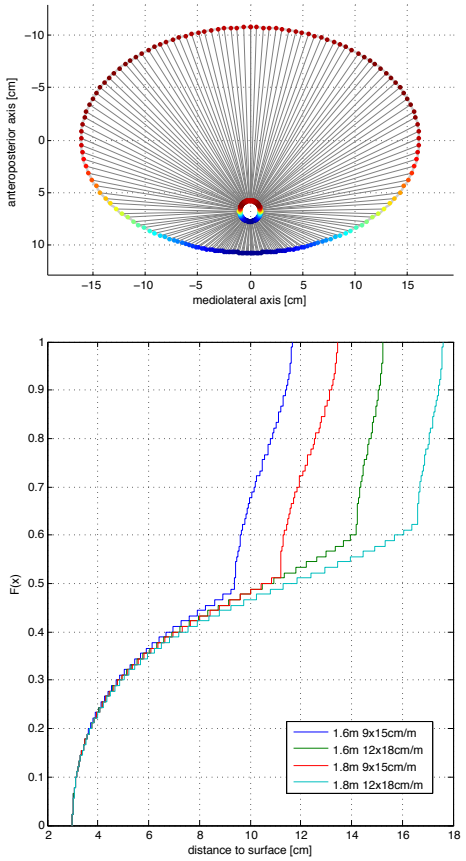

Figure 10: The **upper panel** represents a transverse cross-section through the thorax: the **outer ellipse** is defined by its major and minor axis; the **inner circle**, representing the esophagus, is defined by its diameter and distance from the edge of the ellipse. The **gray lines** emanate radially from the center of the esophagus, thus lying normal to its surface. **Colors** indicate the distance to the skin, which is calculated analytically by solving for the intersection of the line and the ellipse.
The **lower panel** shows the cumulative distribution function of distances to the surface of the skin for 4 different sizes of person. Dimensions in the key give height in meters and major and minor axes of the ellipse per unit of height. Choice of values is based on statistics for 21 male and 19 female subjects in the literature [2], note however that values have been increased slightly to account for the difference in internal and external dimensions. The diameter of the esophagus has been set at 2cm and placed 3cm from the edge of the ellipse (see Figure 3).
This model is provided only to give an indication of the distances in question; in practice, the clinician will have access to scans of the patient from which they can measure the distance.

The second step is to find a magnet which can produce large fields and large gradients. Importantly, however, the magnet need only produce these fields and gradients in a particular region of space. So, as was realized in the 1970s, all that must be done is to assemble a set of separate permanent magnets into a specifically designed structure - known as a Halbach array - which 'focuses' the net magnetic field in a particular region. Coercing the magnets together into the required orientations does require significant force, but once accomplished the magnets can safely be held in place indefinitely with a strong casing. Figure 11 shows a linear Halbach array which projects a strong magnetic field in a half-plane. The size of the individual magnets can easily be configured, however manufacturing arbitrary shapes (such as curved arrays) is more complicated. Thus, here we only consider linear arrays consisting of 1T cubed magnets.[6]

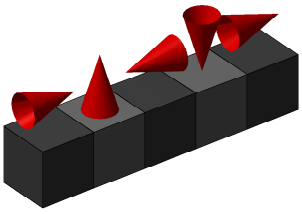

Figure 11: A linear Halbach array composed of five cube permanent magnets. The **red cones** show the direction of the magnetic field in each of the magnets. The magnets are arranged such that the field strength is low in the region below the array, and high in the region above it.

This brings us to the third step, which is to calculate the forces generated by different sized Halbach arrays. The calculation was done using finite element modeling, as discussed in the preceding section,

[6]Simulations [18] were run recently to assess the benefit of using more complex shapes including triangular rods and cylinders. But for magnets of less than 1000 cm^3 it was found that the linear array was - in some section of the field at least - the joint best option. For the geometry examined the volume of the magnet was in fact linearly related to the average force on the particles, up to 1000 cm^3 that is.

and was implemented by the commercial software Opera 3D [22]. The procedure for using the software is a follows:

1. Define the dimensions and relative locations of each magnet.
2. Specify regions of air around the magnet in which to evaluate the field.
3. Define the target mesh size required in each region of the model - for both air and magnets.
4. Provide the B-H curve for the magnets (see Figure 7) and specify their individual orientations.
5. Generate model 'body' from the list of overlapping three dimensional shapes.
6. Run a surface-mesh-generating algorithm.
7. Run a solid-mesh-generating algorithm.
8. Run an algorithmic engine to find an approximation to the static magnetic field (TOSCA).[7]
9. Evaluate $\mathbf{H}$ and $(\mathbf{H} \cdot \nabla)\mathbf{H}$ at the required points, for example on a plane.

Figure 12 gives a visualization of the first few steps in the finite element process. The final calculation of $\mathbf{F}_m$ was performed by importing the data into MATLAB and running a custom script.

An example result is shown in Figures 13, though it makes no attempt to convey the full extent of the three dimensional vector field.

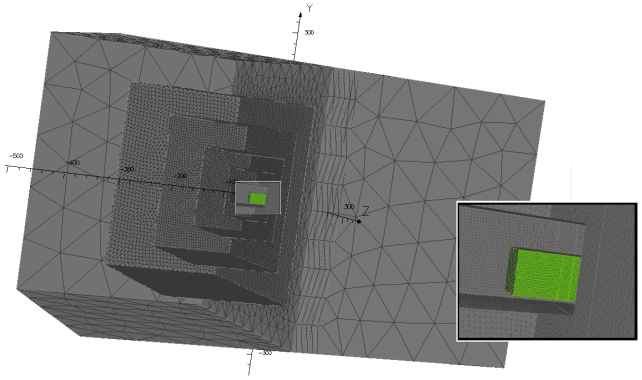

Figure 12: A cutaway showing the mesh used to model a Halbach array of five 2cm-sided cubed 1T magnets. Magenets are shown in **green** and are visible at the centre of the mesh and in the **enlarged insert**. The **gray faces** show the mesh of air surrounding the magnets. Note how the resolution of the mesh has been designed to be of a fine level close to the magnets, and of a more coarse level further from the magnets. The solid mesh is not shown here, only the surface mesh. Axis scales are in mm.

The final stage is to estimate the hydrodynamic drag force acting in opposition to the magnetic force. Hydrodynamic drag, F_d, is given by Stoke's Law:

$$F_d = 6\pi\eta R v \tag{8}$$

where R is the radius of the moving entity, v its velocity, and η the dynamic viscosity of the medium. Other forces may also be relevant, such as those holding the cells to the extracellular matrix, those relating to the motility of cells, gravitation, and fluid-dynamic forces encapsulated by the full Navier-Stokes equation.

Here however we make the approximation that the cells must travel a distance of 2mm through an environment with water-like properties and in which non-hydrodynamic forces can be ignored. Thus, given that cells' density is roughly the same as water we are able to neglect buoyancy (gravity) and in water η is known to be 0.001 Pa·s. Further, if R is taken as approximately 15 μm, we find that $F_d \approx 3v \times 10^{-7}$, and then $v \approx F_m \frac{1}{3} \times 10^7$. Note that equating the drag and magnetic forces ignores acceleration and means that v is actually the terminal velocity. Thus if we wish the cells to travel 2mm in approximately 30 minutes, v should be about 1.5 $\mu m\ s^{-1}$ and F_m must be of the order of 10^{-12} N, i.e. 1 pN.[8]

[7] It is considered good practice to run the meshing and analysis at least twice using different mesh resolutions so that the finite-element errors can be assessed [18]. Here however the mesh sizes were deemed reasonable without this numerical verification.

[8] Forces on the order of 2 pN are quoted in literature as being appropriate in a similar situation [15, 18].

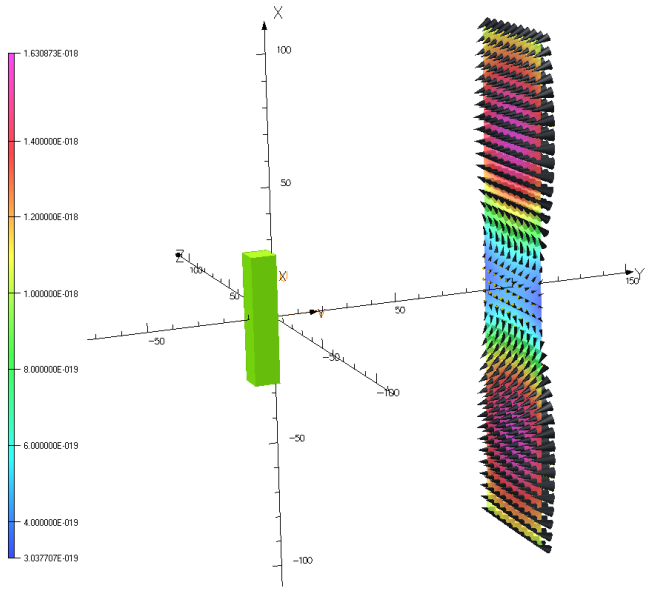

Figure 13: In **green** is a halbach array of five 1cm cubed 1T magnets. The **plane** is positioned 10cm from the magnets and is 20cm long and 5cm wide. The **colours** of the plane are shown in the colorbar and give the magnitude of the force per cell. The black cones show the direction of the force at each point. Forces are in N and correspond to 6 M-450 Dynabeads per cell.

The calculation of forces can easily be computed for a range of different superparamagnetic particles. Figure 15 shows the results for three sizes of Halbach array with M-450 Dynabeads, and Figure 14 compares the forces for three types of particles. The main difference between the three types is the diameter of their iron oxide particles, however they also differ in the maximum non-toxic volume per cell (though this has not been particularly well characterized). Interestingly the figure seems to indicate that these two effects interact to produce different optimum particle types at different field strengths: large (freely moving) particles are toxic at lower concentration but benefit significantly from being more highly magnetized at low field strengths (see also Equation 6).

5 Concluding Remarks

If, as suggested, we require a force of the order 1 pN, then it would appear that a 5×5 cm Halbach array would be sufficient for cells loaded with Dynabeads or 50 nm particles within about 10 cm of the skin. Applying forces to cells more distant from the magnet appears to be difficult. Referring back to Figure 10 this suggests that about half of the esophageal circumference is accessible to this approach.

Thus far we have assumed that the magnetic loading has been applied to the cells, but it would also be possible to tag the extracellular matrix. Perhaps if a synthetic matrix is used it could have a significant loading of superparamagnetic particles. However, assessing the hydrodynamic and internal electromagnetic forces acting on a moving matrix is more complex than the calculation given for individual cells in the preceding section.

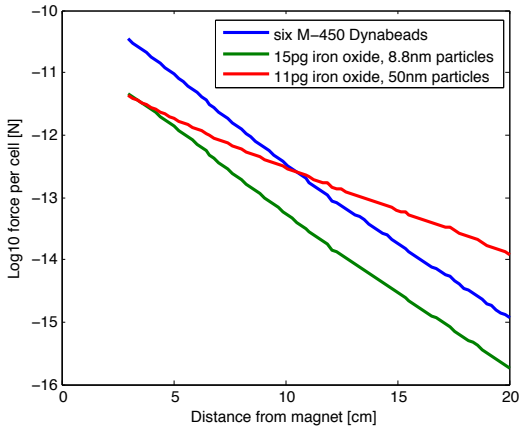

Figure 14: Comparison of force per cell for cells loaded with Dynabeads and cells loaded with simple nanoparticles of iron oxide. Values for Dynabeads taken from [5, 15]; values for 8.8 nm particles taken from [18]. The 50 nm particles are sold by Chemicell (GmbH, Berlin, Germany) and are thought to be non-toxic at a concentration of 11 pg per cell. The **horizontal axis** shows the distance from the magnet along its perpendicular bisector, and the **vertical axis** shows the magnitude of the component of the force pointing back towards the magnet along the bisector. Data is for the 5×5 cm Halbach array.

Previously most studies have focused on delivering magnetically tagged cells via the bloodstream [18, 10] rather than as part of a macroscopic graft. Thus the possibility of applying a force to the matrix has not received much attention. Additionally, much of the work examining the physiological effects of magnetic particles relates to cells and particles in the bloodstream and may not be entirely applicable to cells bound to a matrix that is not in direct contact with the blood (at least initially).[9]

The technique proposed here appears to offer a promising solution to prevent the scarring of the esophagus following resection of cancerous tissue. However much remains to be demonstrated before it is adopted for clinical use. Significantly it is not clear whether sufficient force can be applied to cells more than 10 cm distant from the magnet. An increase in the maximum tolerable load of magnetic particles per cell and an increase in the particle size (while maintaing superparamagnetic properties) may be required. Controlled animal trials that compare magnetically assisted adhesion with simple mechanical adhesion (provided by the endoscope [13]) must also be completed.

References

[1] A. Atala, S.B. Bauer, S. Soker, J.J. Yoo, and A.B. Retik. Tissue-engineered autologous bladders for patients needing cystoplasty. *The Lancet*, 367(9518):1241–1246, 2006.

[2] F. Bellemare, A. Jeanneret, and J. Couture. Sex differences in thoracic dimensions and configuration. *American journal of respiratory and critical care medicine*, 168(3):305–312, 2003.

[3] Invitrogen Dynal Biotech. *The Principles of Dynabeads*. `www.dynalbiotech.com`, 2012.

[4] P.C. Enzinger and R.J. Mayer. Esophageal cancer. *New England Journal of Medicine*, 349(23):2241–2252, 2003.

[5] G. Fonnum, C. Johansson, A. Molteberg, S. Mørup, and E. Aksnes. Characterisation of dynabeads by magnetization measurements and mössbauer spectroscopy. *Journal of magnetism and magnetic materials*, 293(1):41–47, 2005.

[6] U. Galili. The α-gal epitope and the anti-gal antibody in xenotransplantation and in cancer immunotherapy. *Immunology and cell biology*, 83(6):674–686, 2005.

[7] T. Gotoda. Endoscopic resection of early gastric cancer. *Gastric cancer*, 10(1):1–11, 2007.

[8] S. Hsu, I. Tsai, D. Lin, D.C. Chen, et al. The effect of dynamic culture conditions on endothelial cell seeding and retention on small diameter polyurethane vascular grafts. *Medical engineering & physics*, 27(3):267–272, 2005.

[9] M. Knobel, WC Nunes, LM Socolovsky, E. De Biasi, JM Vargas, and JC Denardin. Superparamagnetism and other magnetic features in granular materials: a review on ideal and real systems. *Journal of Nanoscience and Nanotechnology*, 8(6):2836–2857, 2008.

[10] A. Kumar, P.K. Jena, S. Behera, R.F. Lockey, S. Mohapatra, and S. Mohapatra. Multifunctional magnetic nanoparticles for targeted delivery. *Nanomedicine: Nanotechnology, Biology and Medicine*, 6(1):64–69, 2010.

[11] B. Kuo and D. Urma. Esophagus-anatomy and development. *GI Motility online*, 2006.

[12] P. Macchiarini, P. Jungebluth, T. Go, M. Asnaghi, L.E. Rees, T.A. Cogan, A. Dodson, J. Martorell, S. Bellini, P.P. Parnigotto, et al. Clinical transplantation of a tissue-engineered airway. *The Lancet*, 372(9655):2023–2030, 2008.

[13] T. Ohki, M. Yamato, D. Murakami, R. Takagi, J. Yang, H. Namiki, T. Okano, and K. Takasaki. Treatment of oesophageal ulcerations using endoscopic transplantation of tissue-engineered autologous oral mucosal epithelial cell sheets in a canine model. *Gut*, 55(12):1704–1710, 2006.

[14] Q.A. Pankhurst, J. Connolly, SK Jones, and J. Dobson. Applications of magnetic nanoparticles in biomedicine. *Journal of Physics D: Applied Physics*, 36:R167, 2003.

[15] H. Perea, J. Aigner, U. Hopfner, and E. Wintermantel. Direct magnetic tubular cell seeding: a novel approach for vascular tissue engineering. *Cells Tissues Organs*, 183(3):156–165, 2006.

[16] N. Plunkett and F.J. O'Brien. Bioreactors in tissue engineering. *Technology and Health Care*, 19(1):55–69, 2011.

[17] F. Radtke and H. Clevers. Self-renewal and cancer of the gut: two sides of a coin. *Science*, 307(5717):1904, 2005.

[18] J. Riegler, K.D. Lau, A. Garcia-Prieto, A.N. Price, T. Richards, Q.A. Pankhurst, and M.F. Lythgoe. Magnetic cell delivery for peripheral arterial disease: A theoretical framework. *Medical Physics*, 38:3932, 2011.

[9] Magnetic particles in the blood are physiologically inert, but there are a number of proteins that tend to bind to them (opsonization) and make them recognizable to the reticuloendothelial system. This system removes the particles from the blood and either breaks them down or sequesters them in specific organs such as the spleen. Alterations to the particle surface can slow this process, as can drugs that deplete the numbers of cells involved with the uptake process [10]. Some surface coatings actually facilitate uptake by the liver followed by excretion from the body. The smallest nanoparticles (of the order 10 nm) tend to evade uptake by the liver and spleen and are instead sequestered by other cells of the reticuloenothelial system spread throughout the body [14].

[19] T. Samdani, E. Chao, S.M. Greenstein, N.K. Atray, and T.J. Vachharajani. Xenotransplantation. `emedicine.medscape.com/article/432418`, March 2012. Medscape, WebMD.

[20] N.G. Singer and A.I. Caplan. Mesenchymal stem cells: mechanisms of inflammation. *Annual Review of Pathology: Mechanisms of Disease*, 6:457–478, 2011.

[21] Cobham Vector Fields Software. *Opera 3D Reference Manual*, December 2007.

[22] Cobham Vector Fields Software. Opera 3d. `www.cobham.com`, 2011.

[23] R. Takagi, D. Murakami, M. Kondo, T. Ohki, R. Sasaki, M. Mizutani, M. Yamato, K. Nishida, H. Namiki, M. Yamamoto, et al. Fabrication of human oral mucosal epithelial cell sheets for treatment of esophageal ulceration by endoscopic submucosal dissection. *Gastrointestinal endoscopy*, 72(6):1253–1259, 2010.

[24] A. Tavakkolizadeh, U.V. Berger, A.E. Stephen, B.S. Kim, D. Mooney, M.A. Hediger, S.W. Ashley, J.P. Vacanti, and E.E. Whang. Tissue-engineered neomucosa: morphology, enterocyte dynamics, and sglt1 expression topography1. *Transplantation*, 75(2):181, 2003.

[25] Neville Woolf. *Pathology: Basic and Systemic*. Elsevier Health Sciences, 1998.

Acknowledgement. The author is grateful to Richard Day, Quentin Pankhurst, George Frodsham, and Johannes Reigler for their guidance and technical assistance.

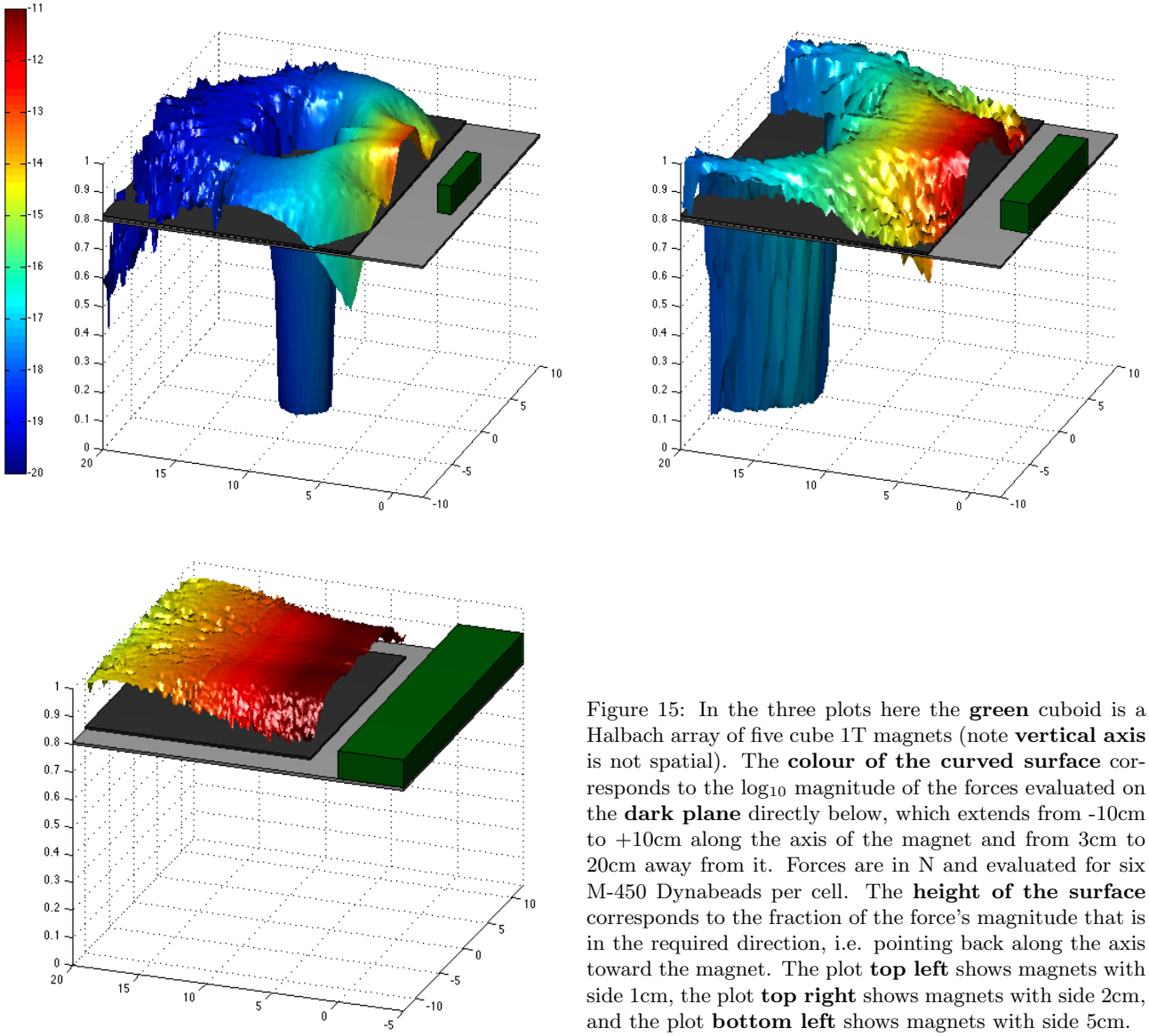

Figure 15: In the three plots here the **green** cuboid is a Halbach array of five cube 1T magnets (note **vertical axis** is not spatial). The **colour of the curved surface** corresponds to the $\log_{10}$ magnitude of the forces evaluated on the **dark plane** directly below, which extends from -10cm to +10cm along the axis of the magnet and from 3cm to 20cm away from it. Forces are in N and evaluated for six M-450 Dynabeads per cell. The **height of the surface** corresponds to the fraction of the force's magnitude that is in the required direction, i.e. pointing back along the axis toward the magnet. The plot **top left** shows magnets with side 1cm, the plot **top right** shows magnets with side 2cm, and the plot **bottom left** shows magnets with side 5cm.